

Regulated Offloading of Cytoplasmic Dynein from Microtubule Plus Ends to the Cortex

Steven M. Markus¹ and Wei-Lih Lee^{1,*}

¹Biology Department, University of Massachusetts Amherst, 221 Morrill South, 611 North Pleasant Street, Amherst, MA 01003, USA

*Correspondence: wlee@bio.umass.edu

DOI 10.1016/j.devcel.2011.04.011

SUMMARY

Cytoplasmic dynein mediates spindle orientation from the cell cortex through interactions with astral microtubules, but neither the mechanism governing its cortical targeting nor the regulation thereof is well understood. Here we show that yeast dynein offloads from microtubule plus ends to the daughter cell cortex. Mutants with an engineered peptide inserted between the tail domain and the motor head retain wild-type motor activity but exhibit enhanced offloading and cortical targeting. Conversely, shortening the “neck” sequence between the tail and motor domains precludes offloading from the microtubule plus ends. Furthermore, chimeric mutants with mammalian dynein “neck” sequences rescue targeting and function. These findings provide direct support for an active microtubule-mediated delivery process that appears to be regulated by a conserved masking/unmasking mechanism.

INTRODUCTION

Cytoplasmic dynein is a 1.2 MDa multisubunit motor complex that powers directional movement of cellular cargoes toward the minus end of microtubule (MT) tracks. This highly conserved motor has been implicated in diverse cellular processes, including vesicular transport, centrosome positioning, and directed cell migration (Burakov et al., 2003; Dujardin et al., 2003). How cells regulate dynein activity with precise spatial and temporal control for each of these distinct functions is poorly understood. One way to regulate dynein activity is by spatially deploying the motor to its sites of action. A well-studied example is the regulated targeting of dynein to kinetochores at early prometaphase in mitotic mammalian cells (Whyte et al., 2008). In this case, dynein recruitment to kinetochores—for checkpoint silencing—depends on the phosphorylation state of the dynein intermediate chain, which specifies its interaction with the kinetochore component *zw10*. Another example of regulated dynein targeting comes from studies in budding yeast, where it has been proposed that dynein exploits the dynamic instability of astral MTs for delivery to its cortical receptor, Num1 (Farkasovsky and Kuntzel, 2001; Heil-Chapdelaine et al., 2000; Lee et al., 2003; Sheeman et al., 2003). Although direct evidence for dynein cortical delivery is lacking, mutations that disrupt

astral MT plus end localization of dynein result in a drastic reduction in cortical dynein (Markus et al., 2009) and a concomitant spindle misorientation defect (Lee et al., 2003; Sheeman et al., 2003). These data imply that dynein must associate with plus ends before it can be targeted to cortical Num1, and raises the question of how dynein is prevented from being directly recruited to cortical sites in the absence of MT plus end localization.

A clue to the mechanism of cortical targeting in yeast came from analysis of cells expressing truncated fragments of the dynein heavy-chain Dyn1 (Markus et al., 2009). Although the motor domain fragment of Dyn1 (Dyn1_{MOTOR}) is necessary and sufficient for plus end targeting, the tail domain (Dyn1_{TAIL}) is responsible for interaction with cortical Num1. Association of Dyn1_{TAIL} with Num1 is very robust, more so than the full-length molecule, and importantly, occurs in a manner that is independent of plus end targeting or the presence of MTs. Based on these results, it was proposed that the cortical association domain within the NH₂-terminal tail is masked by the motor head and that targeting of Dyn1 to plus ends unmasks this region, priming the motor for offloading to cortical Num1.

Here we have further examined the mechanism by which the association between cytoplasmic dynein and cortical Num1 is regulated. By inserting peptide linkers between the NH₂-terminal tail and COOH-terminal motor domains, we have engineered motility-competent mutants that are capable of bypassing the plus ends for association with cortical Num1. Surprisingly, in addition to observing a plus end-independent targeting mechanism, our analysis of the mutants reveals that they are also actively delivered by the plus ends to the cell cortex. Furthermore, in a genetic background where the dynein-dynactin interaction is enhanced, we observed offloading of wild-type dynein to the cortex, indicating that dynactin is limiting in the offloading process. Our findings support the notion that Dyn1 adopts a folded conformation that negatively regulates its association with cortical sites and that this mechanism may be conserved throughout evolution.

RESULTS

Generation of a Constitutively Unmasked Dynein

We postulated that, if intramolecular “masking” of the Dyn1 cortical association domain occurs, such masking would likely depend on a carefully calibrated spatial linkage between the tail and motor domains of the protein. Therefore, we sought to engineer a Dyn1 mutant with a constitutively “unmasked” cortical association domain, by inserting a helix-forming peptide (A(EAAAK)₈A; Arai et al., 2001) into the junction between the tail

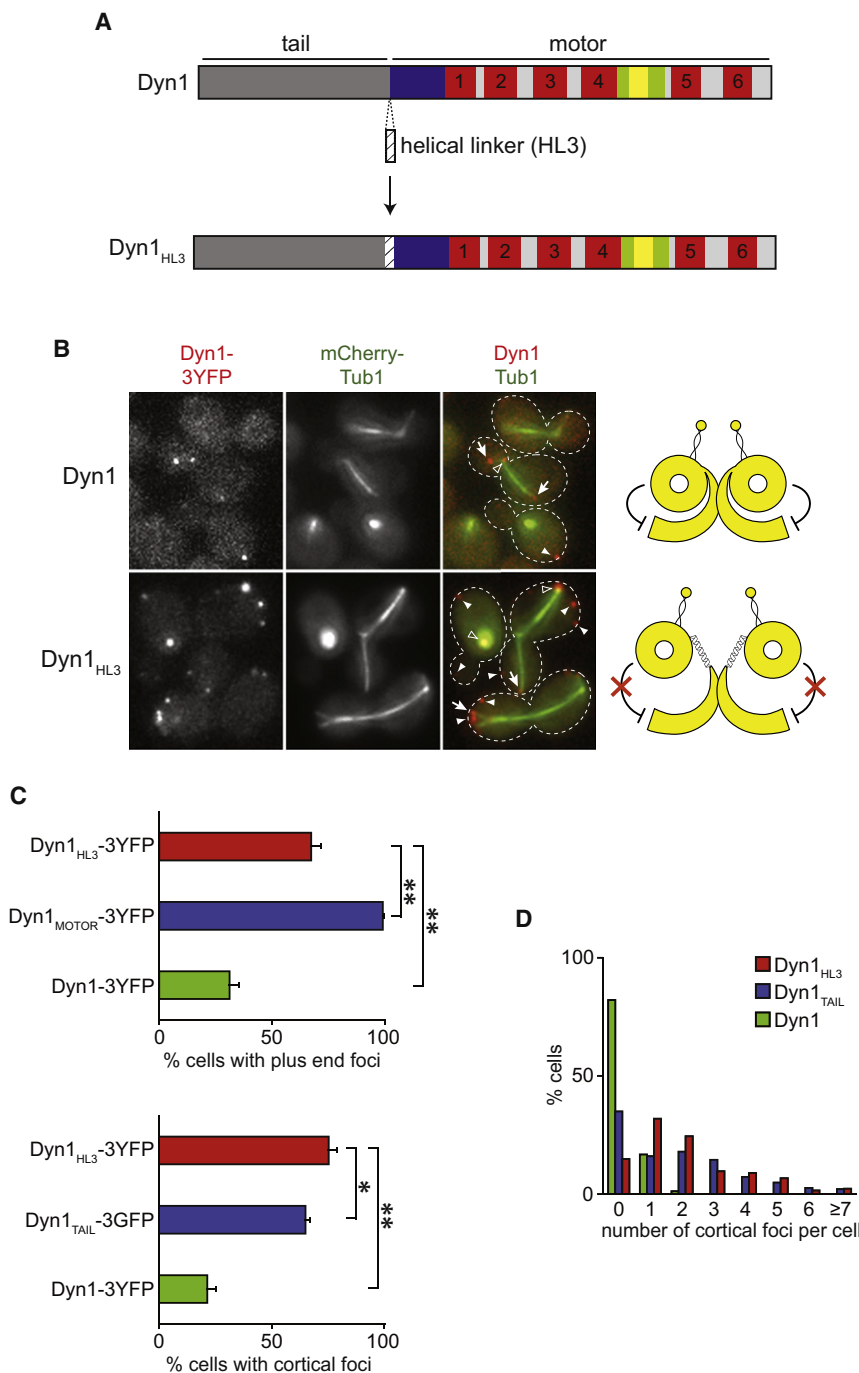


Figure 1. Insertion of a Helical Peptide (HL3) between the Tail and Motor Domains of Dyn1 Enhances Its Plus End and Cortical Targeting

(A) Schematic representation of Dyn1 and the Dyn1_{HL3} mutant, with domain structure of Dyn1 indicated (blue region, “linker” domain defined by in vitro studies (Reck-Peterson et al., 2006); red regions, six AAA domains (Mocz and Gibbons, 2001); green regions, anti-parallel coiled coils of the stalk; yellow region, MT-binding domain (Gee et al., 1997)).

(B) Cells expressing mCherry-Tub1 and either wild-type Dyn1-3YFP (top) or Dyn1_{HL3}-3YFP (bottom). Open arrowheads indicate SPB foci, closed arrowheads show cortical foci, and arrows specify plus end foci. Each image is a maximum intensity projection of a 2 μ m Z stack of wide-field images.

(C) The percentage of cells that exhibit plus end (top) or cortical (bottom) fluorescent foci is plotted for strains expressing mCherry-Tub1 with Dyn1-3YFP, Dyn1_{HL3}-3YFP, Dyn1_{MOTOR}-3YFP, or Dyn1_{TAIL}-3GFP. Stationary cortical foci and motile plus end foci were identified in two-color movies and scored accordingly. Error bars represent standard error of proportion ($n \geq 120$ cells; * $p = 0.0278$; ** $p < 0.0001$).

(D) The percentage of cells exhibiting the indicated number of cortical fluorescent foci is plotted for strains expressing mCherry-Tub1 with Dyn1-3GFP, Dyn1_{HL3}-3YFP, or Dyn1_{TAIL}-3GFP.

and motor domains, creating Dyn1_{HL3} (Figure 1A). We predicted that Dyn1_{HL3} would exhibit (1) cortical targeting reminiscent of Dyn1_{TAIL}-3GFP, and (2) plus end targeting similar to Dyn1_{MOTOR}-3YFP (Markus et al., 2009). We estimate that the inserted peptide has a length of approximately 11.4 nm (Arai et al., 2001), a distance roughly equivalent to the diameter of the motor head (Burgess et al., 2003). We fused a 3YFP or 13myc tag to the COOH terminus of Dyn1_{HL3} for localization and immunoblotting analyses, respectively.

Like wild-type *DYN1*-3YFP cells (Figure 1B, top), *dyn1*_{HL3}-3YFP cells exhibited motile foci associated with spindle pole bodies (SPBs) and MT plus ends, as well as stationary cortical foci (Figure 1B, bottom; see 3D reconstructions in Movie S1 available online). As predicted, the frequency of Dyn1_{HL3}-3YFP targeting to MT plus ends and the cell cortex was significantly greater than Dyn1-3YFP (Figure 1C; 2.2-fold and 3.5-fold, respectively; $p < 0.0001$). Moreover, the number of Dyn1_{HL3}-3YFP cortical foci per cell was elevated with respect to Dyn1-3YFP (Figure 1D). The frequency of plus end targeting for Dyn1_{HL3} was lower than Dyn1_{MOTOR} (Figure 1C; 0.7-fold; $p < 0.0001$), whereas that of cortical targeting was slightly higher than Dyn1_{TAIL} (Figure 1C; 1.2-fold; $p = 0.0278$). As previously described for *DYN1*-3GFP and *dyn1*_{TAIL}-3GFP cells (Markus et al., 2009; Sheeman et al., 2003), plus end and cortical foci in the *dyn1*_{HL3}-3YFP strain exhibited cell cycle-dependent changes in targeting frequencies, most notably as cells entered anaphase (Figure S1A), suggesting similar mechanisms underlying the temporal regulation of their targeting. The differences in plus end and cortical targeting between Dyn1_{HL3} and Dyn1 could not be attributed to altered expression levels or protein stability, as determined by immunoblotting (Figure S1B). Furthermore,

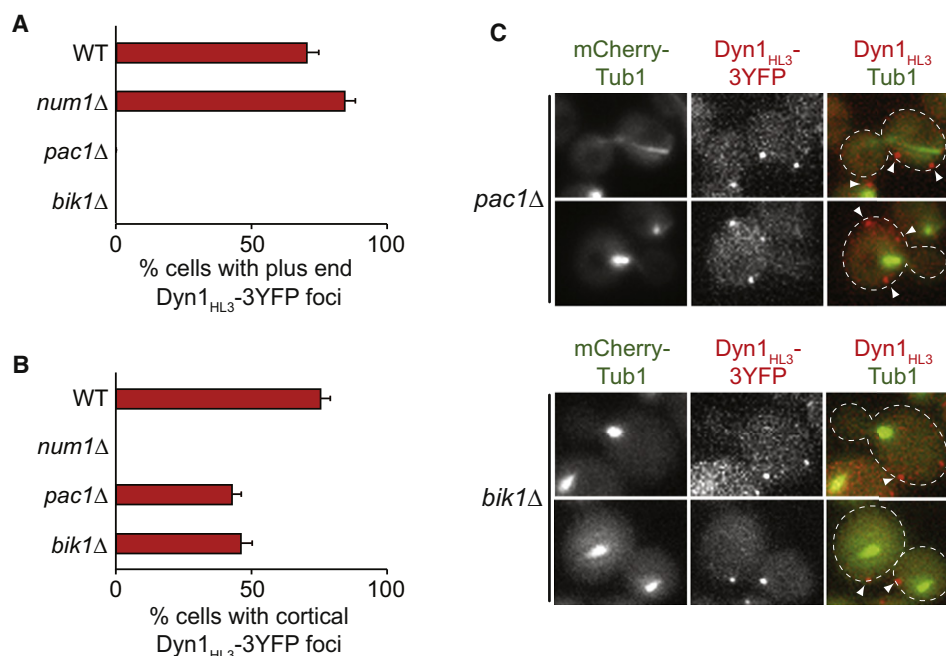


Figure 2. Association of Dyn1_{HL3} with the Cell Cortex Occurs Independently of Plus End Targeting

(A and B) The percentage of cells that exhibit (A) plus end or (B) cortically associated Dyn1_{HL3}-3YFP foci is plotted for wild-type (WT) and indicated null strains ($n \geq 105$ cells). Stationary cortical or motile plus end foci were identified in two-color movies and scored accordingly. Error bars represent standard error of proportion. (C) Representative images of *pac1*Δ or *bik1*Δ cells expressing mCherry-Tub1 and Dyn1_{HL3}-3YFP used for quantitation in (A) and (B). Closed arrowheads indicate cortical Dyn1_{HL3}-3YFP foci. Each image is a maximum intensity projection of a 2 μm Z stack of wide-field images.

13myc-tagged Dyn1_{HL3} and Dyn1 exhibited similar sedimentation profiles in sucrose density gradients (Figure S1C). Although the gradients were unable to resolve any differences in size and shape, the data suggested that Dyn1_{HL3} is assembled into a native complex with its accessory polypeptides. In support of this notion, biochemical isolation of TAP-tagged Dyn1_{HL3} showed that it copurified with the dynein light-intermediate (Dyn3) and intermediate (Pac11) chains to a similar extent as the wild-type TAP-Dyn1 control (Figure S1D). Taken together, these data demonstrate that the observed targeting phenotype is not a result of improper dynein complex assembly or stability.

We next quantitated the extent to which plus end and cortical targeting of Dyn1_{HL3} was dependent on dynein pathway components. Although plus end targeting of Dyn1_{HL3} required the tip-tracking proteins Pac1 (LIS1 homolog) and Bik1 (CLIP-170 homolog), its association with the cortex required the cortical protein Num1 (Figures 2A and 2B; Figure S2B). These results are consistent with Dyn1 (Lee et al., 2003; Sheeman et al., 2003), Dyn1_{MOTOR}, and Dyn1_{TAIL} at each site (Markus et al., 2009). Furthermore, the pattern of Dyn1_{HL3} targeting observed in mutants lacking the dynein accessory chains (Dyn3 or Pac11) or a component of dynactin (Nip100) is more similar to that of Dyn1_{MOTOR} or Dyn1_{TAIL} than the full-length Dyn1 molecule at each site (Figure S2). Most notably, a high percentage of *pac1*Δ (42.7% ± 3.5%) and *bik1*Δ (46.0% ± 4.3%) cells exhibited stationary cortical Dyn1_{HL3}-3YFP foci (Figures 2B and 2C; 3D reconstruction in Movie S2). This finding contrasts with Dyn1, which exhibited a loss of cortical foci in the same mutant strains (Markus et al., 2009). These data indicate that insertion of the

helical linker enables Dyn1 to bypass the plus end for targeting to the cell cortex.

Direct Observation of Dynein Offloading to the Cell Cortex

Although Dyn1_{HL3} does not require plus end targeting to associate with the cortex, we observed that a significantly greater percentage of cells exhibited cortical Dyn1_{HL3}-3YFP foci when the plus end-targeting mechanism was functional (i.e., in WT versus *pac1*Δ or *bik1*Δ backgrounds; Figure 2B; 1.8-fold and 1.6-fold, respectively; $p < 0.0001$). Furthermore, several mutants with disrupted cortical targeting (*num1*Δ, *pac11*Δ, and *nip100*Δ) exhibited an enhancement of Dyn1_{HL3}-3YFP at MT plus ends (Figure S2C). Together, these data suggest that, in addition to direct recruitment from the cytosol, Dyn1_{HL3} might also be actively delivered to the cell cortex from the plus ends of astral MTs. Such delivery (offloading) has been previously proposed (Lee et al., 2003, 2005; Markus et al., 2009; Sheeman et al., 2003), but direct evidence has remained elusive. We investigated whether Dyn1_{HL3} can be observed undergoing offloading.

Strikingly, two-color time-lapse imaging of mCherry-Tub1 and Dyn1_{HL3}-3YFP revealed that Dyn1_{HL3} is indeed offloaded from the plus ends of astral MTs to the cell cortex (Figures 3A and 3B, left; Figures S3C and S3D and Movie S3). Intensity measurements of plus end Dyn1_{HL3}-3YFP at the moments preceding and following the offloading events revealed that the majority of Dyn1_{HL3}-3YFP was delivered to the cell cortex (Figure 3A, right). Analysis of 27 offloading events revealed that the majority occurred in daughter cells during anaphase (Figures S3A and

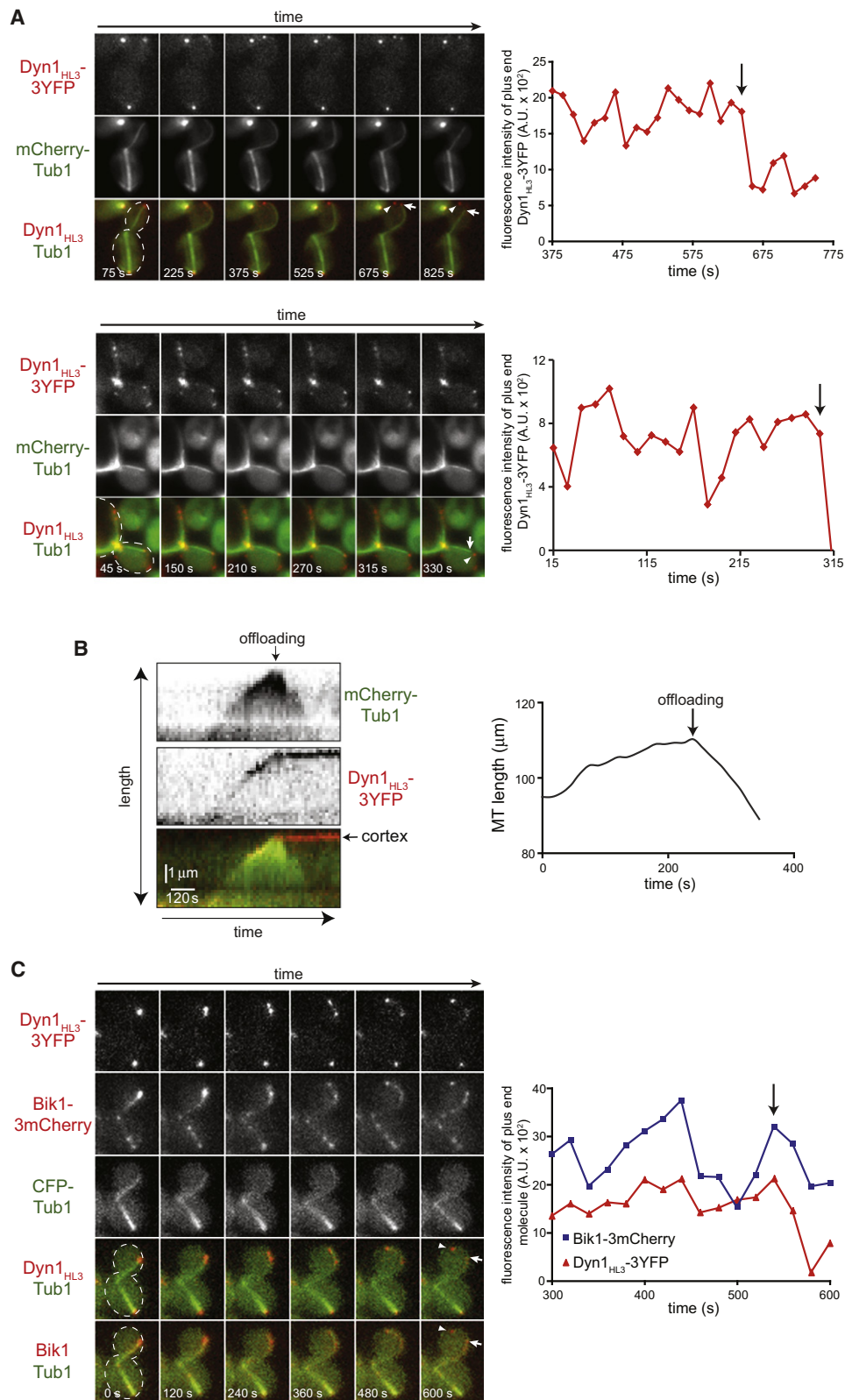


Figure 3. Direct Observation of Dyn1_{HL3} Offloading from MT Plus End to the Cell Cortex

(A) Representative movie frames of cells expressing Dyn1_{HL3}-3YFP and mCherry-Tub1. Arrowheads show offloaded Dyn1_{HL3}, and arrows indicate MT plus end following offloading event. Graphs depict fluorescence intensity of plus end-associated Dyn1_{HL3}-3YFP at the moments preceding and directly following an offloading event (vertical arrows). Each image is a maximum intensity projection of a 2 μ m Z stack of wide-field images. Also see [Movie S3](#) and [Figure S3C](#).

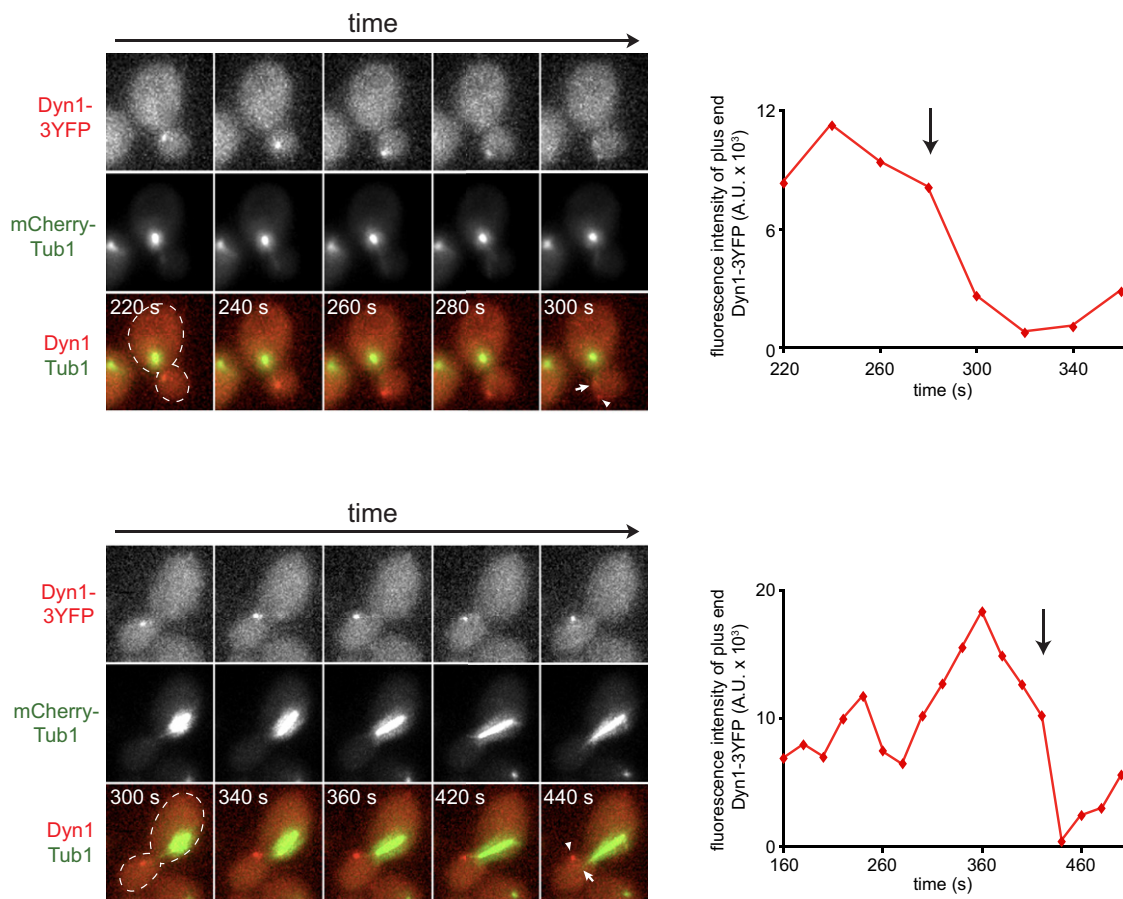


Figure 4. Direct Observation of Wild-Type Dyn1 Offloading from MT Plus End to the Cell Cortex

Representative movie frames of *she1Δ* cells expressing Dyn1-3YFP and mCherry-Tub1. Arrowheads indicate offloaded Dyn1, and arrows show MT plus end following offloading event. Graphs depict fluorescence intensity of plus end-associated Dyn1-3YFP at the moments preceding and directly following an offloading event (vertical arrows). Each image is a maximum intensity projection of a 2 μ m Z stack of wide-field images. Also see [Movie S4](#).

S3B). Furthermore, we noted that immediately following offloading, the majority of astral MTs (96%) underwent catastrophe ([Figure 3B](#), right, and [Figure S3D](#)). These observations show that dynein does in fact utilize an offloading mechanism for cortical targeting. To our knowledge, they represent the first demonstration that a cellular motor exploits the dynamic instability of astral MTs for delivery to its site of action.

We recently showed that the dynactin complex, which is required for cortical dynein localization ([Lee et al., 2003](#)), is limiting at MT plus ends with respect to dynein (one dynactin to three dynein complexes; [Markus et al., 2011](#)). We predicted that enhancing the dynactin:dynein ratio at MT plus ends would enable us to visualize the offloading of wild-type dynein to the cell cortex. To this end, we generated a yeast strain lacking a regulator of dynactin-dynein binding at MT plus ends, *She1*

([Woodruff et al., 2009](#)). Cells lacking *She1* exhibit a dynactin:dynein ratio at MT plus ends that is close to 1:1 ([Markus et al., 2011](#)). Strikingly, as predicted, time-lapse imaging of mCherry-Tub1 and Dyn1-3YFP in *she1Δ* cells revealed that wild-type Dyn1 is also offloaded from MT plus ends to the cell cortex ([Figure 4](#); [Movie S4](#)). Analysis of 16 Dyn1-3YFP offloading events revealed that the majority occurred in daughter cells (15 of 16), whereas all events took place during preanaphase. These data are consistent with the notion that the association of dynactin with plus end-associated dynein is a limiting step in the offloading process.

In budding yeast, cortical dynein drives the sliding of astral MTs along the cell cortex ([Adames and Cooper, 2000](#)). However, we did not observe such activity following any of the Dyn1_{HL3} offloading events. Furthermore, *dyn1_{HL3}-3YFP* cells had a level of

(B) Kymograph depicting a Dyn1_{HL3} offloading event and a life history plot of the same MT leading up to and immediately following the offloading event (also see [Figure S3D](#)). Merge image in kymograph shows mCherry-Tub1 in green and Dyn1_{HL3}-3YFP in red. MT lengths were measured using ImageJ from two-dimensional projections of 2 μ m Z stacks of wide-field fluorescence images. The time at which offloading occurred is indicated on the kymograph and the life history plot by the vertical arrow.

(C) Similar to (A) but with cells expressing Dyn1_{HL3}-3YFP, Bik1-3mCherry, and CFP-Tub1. Graph depicts fluorescence intensity of plus end-associated Dyn1_{HL3}-3YFP (red) and Bik1-3mCherry (blue). Also see [Movie S5](#), top.

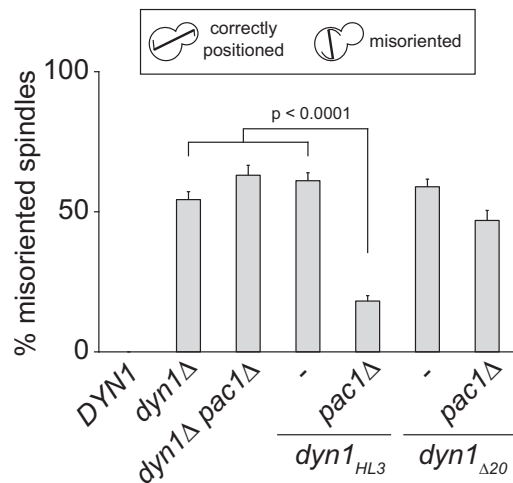


Figure 5. In Vivo Functional Assessment of Dyn1 Neck Mutants

The percentage of cells with a misoriented mitotic spindle in a cold (16°C) spindle position assay (Lee et al., 2005; Li et al., 2005) is plotted for haploid strains carrying *DYN1*-3YFP (indicated as *DYN1*), *dyn1Δ*, *dyn1Δ pac1Δ*, *dyn1_{HL3}*-3YFP (indicated as *dyn1_{HL3}*), *dyn1_{HL3}*-3YFP *pac1Δ*, *dyn1_{Δ20}*-3YFP (indicated as *dyn1_{Δ20}*), and *dyn1_{Δ20}*-3YFP *pac1Δ*. Spindles were visualized using mCherry-Tub1. Strains were imaged after growth at 16°C to mid-log phase in synthetic-defined media lacking methionine (to induce mCherry-Tub1 expression controlled by the *MET3* promoter). Error bars represent standard error of proportion ($n \geq 184$ cells for each strain). Student's *t* test was used to calculate *p* values.

spindle misorientation that was comparable to that of a dynein null strain (Figure 5), suggesting that motor activity is compromised in this mutant (see more results below).

Plus End-Targeting Components Ectopically Colocalize with Cortical Dyn1_{HL3}-3YFP

We used functionally tagged fluorescent proteins (Markus et al., 2011) to assess the localization of dynein pathway components with respect to cortical Dyn1_{HL3}-3YFP. As previously described for cortical Dyn1_{TAIL}-3GFP foci (Markus et al., 2009), cortical Dyn1_{HL3}-3YFP foci colocalized with Num1-mCherry, the dynein intermediate chain Pac11-3mCherry, and the dynactin subunit dynactin Jnm1-3mCherry (Figures S4A–S4C). The frequency with which cortical Pac11-3mCherry and Jnm1-3mCherry foci were observed in *dyn1_{HL3}*-3YFP cells was enhanced significantly with respect to wild-type *DYN1* cells (Jnm1: from 6.6% ± 1.8% to 73.5% ± 6.3%; Pac11: from 13.0% ± 1.8% to 86.8% ± 3.0%; $n \geq 49$ cells; $p < 0.0001$). Because cortical targeting of both Pac11 and dynactin depend on Dyn1 (Lee et al., 2005; Moore et al., 2008), these data indicate that both are recruited to the cortex in complex with Dyn1_{HL3}-3YFP.

Compared to wild-type (*DYN1*) cells, *dyn1_{HL3}*-3YFP cells exhibited similar localization patterns and expression levels of Num1 (Figures S5A and S5B), indicating that the enhanced cortical targeting of Dyn1_{HL3} is not due to changes in the dynein cortical receptor. However, we observed an enhanced association between Dyn1_{HL3} and Num1, as assessed by the bimolecular fluorescence complementation assay (BiFC; Hu et al., 2002). VN-Dyn1_{HL3} and VC-Num1 (Figure S5) expressing cells

possessed brighter and a significantly greater number of cortical BiFC foci than those expressing VN-Dyn1 and VC-Num1 (Figures S5C and S5D). These observations are consistent with the presence of a higher-order complex of Dyn1_{HL3} with various dynein and dynactin components at the cell cortex.

We found that, in contrast to cortical Dyn1 (depicted in Figure 6I), cortical Dyn1_{HL3}-3YFP colocalized with four components required for dynein plus end targeting (Carvalho et al., 2004; Lee et al., 2003; Sheeman et al., 2003) (S. Markus and W.-L. Lee, unpublished data), namely Dyn3-3mCherry, Pac1-3mCherry, Bik1-3mCherry, and the kinesin Kip2-mCherry (Figures 6A–6D and 6I). However, another tip-tracking protein, Bim1-3mCherry, the EB1 homolog, was not found at the cortex in *dyn1_{HL3}*-3YFP cells, consistent with its noninvolvement in the budding yeast dynein pathway (Carvalho et al., 2004) (Figure S4D). Dyn3 associates with the tail domain (Figure S4E), whereas our previous work (Markus et al., 2009) suggested that Pac1, Bik1, and Kip2 likely associate with the motor domain of Dyn1_{HL3} (Figure 6I). Because Pac1 binds with higher affinity to Dyn1_{MOTOR} than to full-length Dyn1 (Markus et al., 2009), we tested whether Pac1 would exhibit an enhanced interaction with Dyn1_{HL3}. As expected, and consistent with being unmasked, TAP-tagged Dyn1_{HL3} pulled down more Pac1-13myc as compared to wild-type TAP-Dyn1 (Figure 6E; 5.6-fold when normalized to levels of purified Dyn1; see Figure 6E legend). We conclude that all four of the plus end-targeting components (Dyn3, Pac1, Bik1, and Kip2) are recruited to the cortex in complex with Dyn1_{HL3}-3YFP, given that they are found exclusively associated with MTs and are absent from the cortex of wild-type cells (Carvalho et al., 2004; Lee et al., 2003, 2005; Lin et al., 2001).

In support of this conclusion, three-color time-lapse imaging of CFP-Tub1, Dyn1_{HL3}-3YFP, and either Bik1-3mCherry or Pac1-3mCherry revealed that both Bik1 and Pac1 are offloaded from MT plus ends to the cell cortex together with Dyn1_{HL3}-3YFP (Figure 3C; Movie S5). These data demonstrate that the dynein plus end-targeting components are recruited to the cell cortex in part through offloading as a cocomplex with Dyn1_{HL3}-3YFP.

We asked whether the abnormal association of cortical dynein with Pac1, Bik1, and Kip2 accounts for the lack of dynein function observed in the *dyn1_{HL3}*-3YFP strain. Because deletion of Pac1 resulted in a loss of cortical Bik1 (Figure 6F; but not vice versa, Figure 6G) and Kip2 (Figure S4F), but not cortical dynactin (Figure 6H), we used a *pac1Δ* mutant to assess the function of Dyn1_{HL3}-3YFP. Interestingly, the spindle misorientation defect noted in the *dyn1_{HL3}*-3YFP strain was partially rescued by loss of Pac1 (Figure 5), suggesting that association of cortical dynein with the plus end-targeting machinery may be a causal factor for defective activity. Because loss of Dyn3 resulted in defective Dyn1_{HL3}-3YFP cortical targeting (Figures S2A and S2B), we were unable to determine the consequence of cortical Dyn3 on in vivo dynein function.

Single-Molecule Analysis Reveals that Dyn1_{HL3} Is a Processive Motor and that Pac1 Reduces Dynein Velocity

To further investigate the motor function of Dyn1_{HL3}, we purified full-length Dyn1_{HL3}-GFP and wild-type Dyn1-GFP from yeast using an NH₂-terminal TAP tag, and examined their motile

behavior in vitro at single-molecule resolution using time-lapse total internal reflection fluorescence (TIRF) microscopy (Figure S6A). We verified that we were observing single molecules by quantitating stepwise photobleaching of purified GFP particles (Figures S6B and S6C). The maximum number of bleaching events observed for any fluorescent particle was two, for both Dyn1_{HL3}-GFP and Dyn1-GFP, consistent with the obligatory dimeric nature of motile dynein (Reck-Peterson et al., 2006). Single Dyn1-GFP molecules traveled along MTs with an average velocity of 75.4 nm/s and an average run length of 3.8 μ m (Figure 7A), values close to that previously described for TMR-labeled yeast cytoplasmic dynein (Cho et al., 2008; Kardon et al., 2009; Reck-Peterson et al., 2006). Interestingly, single molecules of Dyn1_{HL3}-GFP also exhibited processive movement along MTs; however, they moved significantly slower than wild-type Dyn1-GFP (Figure 7A; 38.8 nm/s). To determine whether the reduced velocity of Dyn1_{HL3}-GFP was due to an enhanced association with the plus end-targeting machinery (Figure 6), we purified Dyn1-GFP and Dyn1_{HL3}-GFP from cells lacking either Bik1 or Pac1. Strikingly, Dyn1_{HL3}-GFP isolated from a *pac1 Δ* strain (Figure 7C; Movie S7), but not *bik1 Δ* (Figure 7B; Movie S6), exhibited a mean velocity (67.5 ± 41.2 nm/s) very similar to wild-type Dyn1-GFP (67.2 ± 41.2 nm/s), with a slightly reduced run length (2.3 ± 0.2 μ m versus 3.2 ± 0.2 μ m). These data are consistent with the spindle misorientation assay (Figure 5), and suggest that Pac1, which copurifies with Dyn1_{HL3} even in the absence of Bik1 (Figure 6E), is a potent negative regulator of dynein motility.

Insertion versus Removal of Amino Acids at the Tail/Motor Junction Produces Opposite Dynein-Targeting Phenotypes

We next asked whether linkers of different lengths and properties could enable Dyn1 to bypass the plus end for association with the cell cortex. We inserted shorter helix-forming or flexible linkers (Arai et al., 2001) into the tail/motor junction along with a COOH-terminal 3YFP tag. To our surprise, all linkers tested, including a single alanine (Dyn1_{Ala}-3YFP) or proline (Dyn1_{Pro}-3YFP) insertion, were sufficient to cause a phenotype consistent with a constitutively unmasked state. Cortical targeting for Dyn1_{Ala}-3YFP was indistinguishable from Dyn1_{HL3}-3YFP in both *PAC1* and *pac1 Δ* cells (Figure 8C; data not shown).

To test whether the unmasked phenotype is specifically elicited by peptide insertions, we deleted a 20 amino acid sequence spanning the tail/motor junction (Figure 8A) and determined its effects on Dyn1 localization and function. Like wild-type Dyn1 and the insertion mutants, Dyn1 _{Δ 20}-3YFP localized to SPBs and astral MT plus ends; however, this mutant also localized along the length of astral MTs (Figure 8B, top) and was found at the cell cortex in only $4.9\% \pm 1.6\%$ of cells (compared to $21.4\% \pm 3.9\%$ for Dyn1-3YFP; Figure 8C). Furthermore, deletion of Pac1 resulted in a complete loss of Dyn1 _{Δ 20}-3YFP from plus ends and the cell cortex ($n = 141$ cells; Figure 8B, bottom), suggesting that Dyn1 _{Δ 20}-3YFP could not be directly recruited from the cytosol to the cell cortex, a result consistent with a masked phenotype. Additionally, a *dyn1 Δ 20*-3YFP mutant and a *dyn1 Δ 20*-3YFP *pac1 Δ* double mutant exhibited levels of spindle misorientation comparable to a *dyn1 Δ* mutant and a *dyn1 Δ* *pac1 Δ* double mutant (Figure 5). Together, these data suggest

that Dyn1 _{Δ 20}-3YFP exhibits properties indicative of a constitutively masked state.

Conservation of Structure Function within the Dynein “Neck” Region

Previous structural analyses of the dynein heavy chain (Burgess et al., 2004; Meng et al., 2006) have revealed a great degree of flexibility—both planar and torsional—at the junction between the tail and motor domains. The pivot point for this flexibility is situated within the “neck,” the region targeted for mutagenesis in our study. Secondary structure prediction of this region revealed a high probability of α -helical content that is strongly conserved among *S. cerevisiae*, *S. pombe*, and *R. norvegicus*, despite a fairly low similarity in primary sequence (Figures S7A and S7B). Moreover, we noted that the number of amino acids within this region is invariant across species, with no gaps observed in a 219 amino acid stretch (Figure S7C, red underline), suggesting that the length of the region spanning the tail/motor junction is important for dynein function. Because altering this region had little effect on motor activity as demonstrated by the in vitro motility assays, we deduced that this region may be important for the proper targeting of dynein.

Given the highly conserved α -helical pattern of the neck region (Figure S7A), we asked whether a neck sequence from the rat dynein heavy chain could functionally substitute for the corresponding region in yeast Dyn1. We replaced a 10 or 20 amino acid stretch spanning the tail/motor junction of Dyn1 (amino acids 1359–1368 or 1354–1373) with the corresponding rat sequence, generating Dyn1_{rat10}-3YFP and Dyn1_{rat20}-3YFP, respectively (Figure 8D). We found that the plus end and cortical targeting for Dyn1_{rat10}-3YFP and Dyn1_{rat20}-3YFP were comparable to wild-type Dyn1-3YFP (Figure 8E). Furthermore, both chimeras fully rescued dynein function, as determined by a spindle misorientation assay (Figure 8F). These data indicate that the secondary structure of the neck, but not the primary sequence per se, is important for Dyn1 targeting and function. They further suggest a conservation of the mechanism regulating the subcellular targeting of the dynein complex.

DISCUSSION

In summary, we have characterized the mechanism of Dyn1 cortical targeting via offloading from MT plus ends. Importantly, the length of the “neck” linking the motor head and cortex-targeting tail domains is a critical determinant of this mode of Dyn1 targeting. Increasing neck length not only promotes plus end-Dyn1 offloading to the cortex, and indeed permits cortical binding independent of prior localization to plus ends, but also enhances the association of cortical Dyn1 with plus end-protein partners. These findings suggest that the increase in neck length unmasks the heavy chain of yeast cytoplasmic dynein to permit promiscuous association with diverse partners, including Pac1 and Num1. Because shortening the neck conversely stabilizes Dyn1 at plus ends and precludes its offloading to the cortex, we propose that Dyn1 normally utilizes this masking/unmasking mechanism to regulate its subcellular localization. In vitro motility assays revealed that amino acid insertion into the dynein neck region, which is invariant in length across species, does not disrupt MT binding or motor activity, suggesting that the

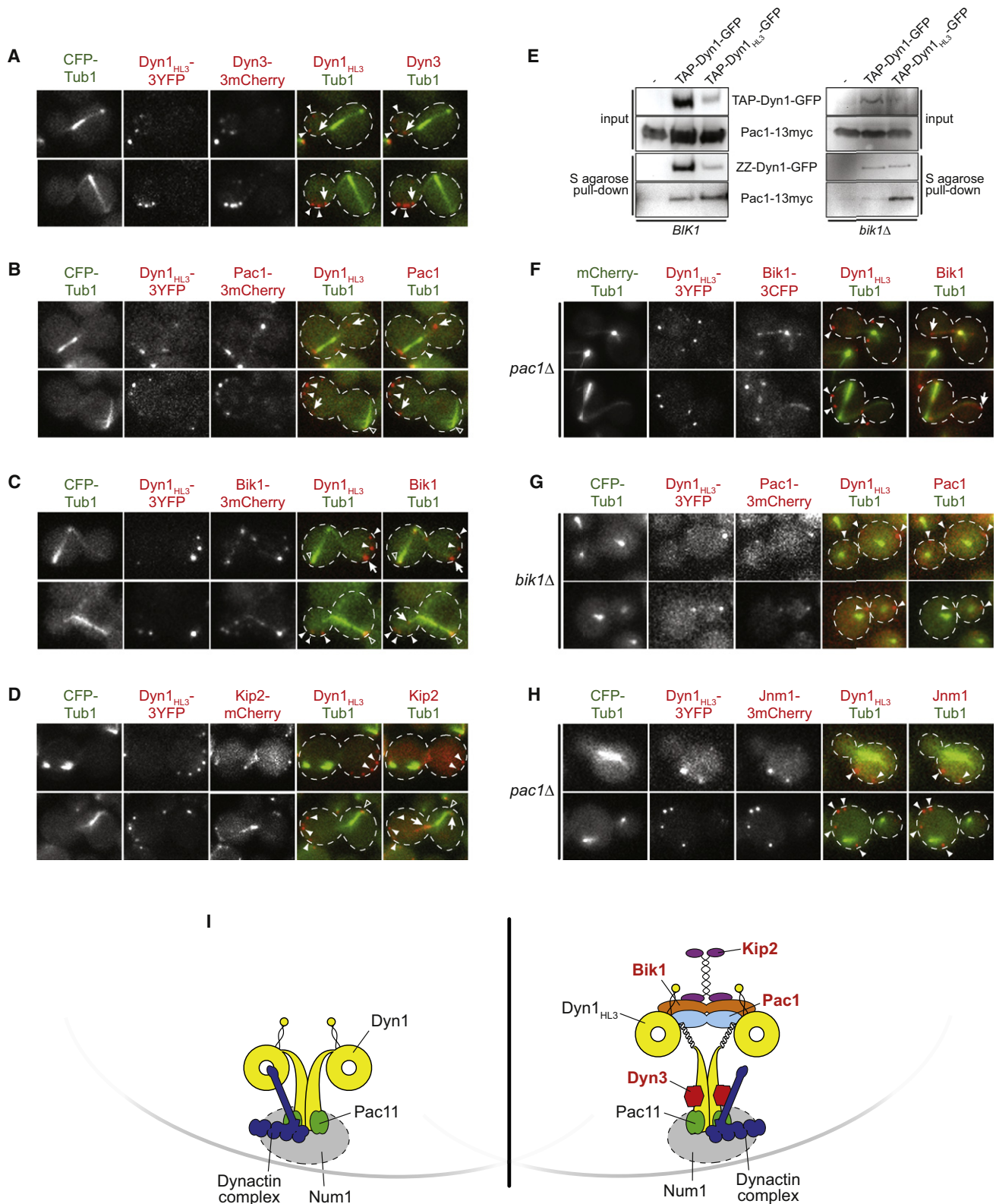


Figure 6. Dyn1_{HL3}-Expressing Cells Exhibit Ectopic Cortical Dyn3, Pac1, Bik1, and Kip2

(A–D) Wide-field fluorescence images of *dyn1_{HL3}-3YFP* cells expressing (A) Dyn3-3mCherry, (B) Pac1-3mCherry, (C) Bik1-3mCherry, or (D) Kip2-mCherry. (E) TAP-tagged Dyn1_{HL3}-GFP pulls down more Pac1-13myc compared to wild-type Dyn1-GFP, in the presence (left; *BIK1*) and absence (right; *bik1Δ*) of Bik1. Equal amounts of protein lysate were incubated with S protein agarose. Bound proteins were released by TEV protease digestion and immunoblotted with rabbit

observed in vivo cortical-targeting phenotype is not due to compromised motor activity but that this region instead has a specific role in regulating dynein targeting. Furthermore, the ability of a neck sequence from a vertebrate dynein heavy chain to functionally substitute for the corresponding region in Dyn1 suggests a conservation of structure and function across species, and suggests that a similar mechanism may exist to regulate dynein targeting in higher eukaryotes.

The regulation of Dyn1 targeting to the cell cortex is likely crucial to spatially and temporally restrict dynein activity. Consistent with this idea, we previously showed that association of Dyn1 with the cell cortex is enhanced as cells approach anaphase (Markus et al., 2009). Similarly, cortical targeting of dynein-dynactin in mammalian cells appears to be temporally restricted to prometaphase and metaphase (Busson et al., 1998; Kobayashi and Murayama, 2009), suggesting that a similar mechanism may be in place to regulate cortical dynein. Our observations define a strategy by which dynein can restrict its own spatial targeting and support an emerging view that dynein activity can be regulated by its spatial deployment. Because purified dynein is active for processive movement along MTs, it has been proposed that its specificity of action is accomplished by cofactor-mediated inhibition, rather than activation (Kardon and Vale, 2009); however, to our knowledge, no such inhibitor has yet been identified. By precisely restricting dynein targeting to its site of action, the need to regulate its motor activity is minimized. It is interesting to note that the majority of Dyn1 offloading events occurred within the daughter cell, regardless of whether the protein was mutated. This bias may be a result of upstream events regulating plus end recruitment of dynein (Grava et al., 2006) and may have implications for the targeting of polarity factors during asymmetric cell division.

Using purified Dyn1_{TAIL} and Dyn1_{MOTOR}, we were unable to detect an interaction between the two domains in solution because they migrated independently in a sucrose gradient (S. Markus and W.-L. Lee, unpublished data). Because the putative unmasking process can be triggered by the insertion of a single amino acid (i.e., Dyn1_{Ala}-3YFP and Dyn1_{Pro}-3YFP), it seems plausible that any potential interaction may be weak and, thus, difficult to detect. Additionally, it is possible that the interaction is either inhibited by a copurifying factor or mediated by a cofactor that is absent from the purification. As an example of the latter, an interaction between the Dam1 and Ndc80 kinetochore complexes could only be detected in the presence of MTs (Lampert et al., 2010). However, our data are not consistent with the tail-motor interaction being mediated by MTs because disruption of Dyn1 plus end association (i.e., in *pac1Δ* or *bik1Δ* strains; Markus et al., 2009) results in a loss of cortical dynein due to the adoption of a masked state. Alternatively, it is possible

that there is no direct interaction between these two domains. Rather, the masked state may be mediated by a folded conformation resulting from a bending within the neck of the heavy chain. Previous structural analyses of dynein have revealed the potential for such conformational changes as a result of the flexibility situated within the neck region (Burgess et al., 2004; Meng et al., 2006).

Other motors, such as kinesin (Cai et al., 2007; Coy et al., 1999; Friedman and Vale, 1999; Hackney et al., 1992; Seiler et al., 2000; Stock et al., 1999; Verhey et al., 1998) and myosin (Krementsov et al., 2004; Pasternak et al., 1989; Stoffler and Bahler, 1998; Wang et al., 2004), undergo intramolecular interactions to modulate their enzymatic activity. In both cases, the COOH-terminal tail domain inhibits the ATPase activity of the NH₂-terminal motor head. Upon cargo binding (or Ca²⁺, in the case of myosin), the motor head exhibits enhanced ATPase activity and becomes activated for track binding. Nish-iura et al. (2004) found that a dynein motor domain construct from *Dictyostelium* possessed a significantly higher MT-stimulated ATPase activity than full-length bovine dynein. Whether this is attributable to species-specific variation or to the monomeric (motor fragment) versus dimeric (full-length) states is unknown. However, the authors proposed the possibility that the tail domain may suppress the ATPase cycle of the dynein motor. Here we provide evidence that a similar yet distinct process is taking place: the motor domain is precluding the tail domain from binding to cortical Num1.

The specific event that triggers unmasking is unknown but may involve the association of dynactin with plus end-bound dynein. Although dynein is targeted to MT plus ends independently of dynactin in yeast, the association of dynein with the cell cortex is dependent upon dynactin (Lee et al., 2003; Moore et al., 2008; Sheeman et al., 2003). Furthermore, we recently showed that dynactin at plus ends is limiting with respect to dynein (one dynactin complex per approximately three dynein complexes; Markus et al., 2011), and work from another lab showed that She1, a regulator of dynein activity, may actively preclude this association (Woodruff et al., 2009). In support of this hypothesis, we have observed here that wild-type Dyn1 offloads to the cell cortex in cells lacking She1. In *she1Δ* cells, the dynactin:dynein ratio is increased to 1:1 (Markus et al., 2011). As a result, *she1Δ* cells have been seen to exhibit hyper-cortical dynein activity (Markus et al., 2011; Woodruff et al., 2009). These data are consistent with the notion that the binding of dynactin to plus end dynein triggers the unmasking of the cortical association domain situated within the dynein tail domain.

The differential motile properties of Dyn1_{HL3}-GFP purified from *bik1Δ* and *pac1Δ* strains indicate that the LIS1 homolog, Pac1, which copurifies with Dyn1_{HL3} even in the absence of Bik1

IgG (for ZZ-Dyn1-GFP or ZZ-Dyn1_{HL3}-GFP) or anti-c-Myc (for Pac1-13myc). The yield of ZZ-Dyn1_{HL3}-GFP from cell lysate was consistently less than that for wild-type ZZ-Dyn1-GFP (left, middle, and right lanes; also see Figure S1D). Upon deletion of Bik1 (right) or Pac1 (not shown), recovery of ZZ-Dyn1_{HL3}-GFP was improved to a level comparable to that for wild-type ZZ-Dyn1-GFP.

(F and G) Cortical Bik1 is lost in *dyn1_{HL3}-3YFP pac1Δ* cells, but Pac1 is retained at the cortex in *dyn1_{HL3}-3YFP bik1Δ* cells.

(H) Colocalization of the dynactin subunit dynamitin Jnm1 with cortical Dyn1_{HL3} in *pac1Δ* cells. All images are maximum intensity projections of a 2 μm Z stack of wide-field fluorescence images. Open arrowheads show SPB foci, closed arrowheads indicate cortical foci, and arrows specify plus end foci.

(I) Schematic drawings of wild-type (left) and Dyn1_{HL3} (right) cortical dynein complexes. Kip2, Bik1, Pac1, and Dyn3 (labeled in red) are not found at the cell cortex in wild-type cells.

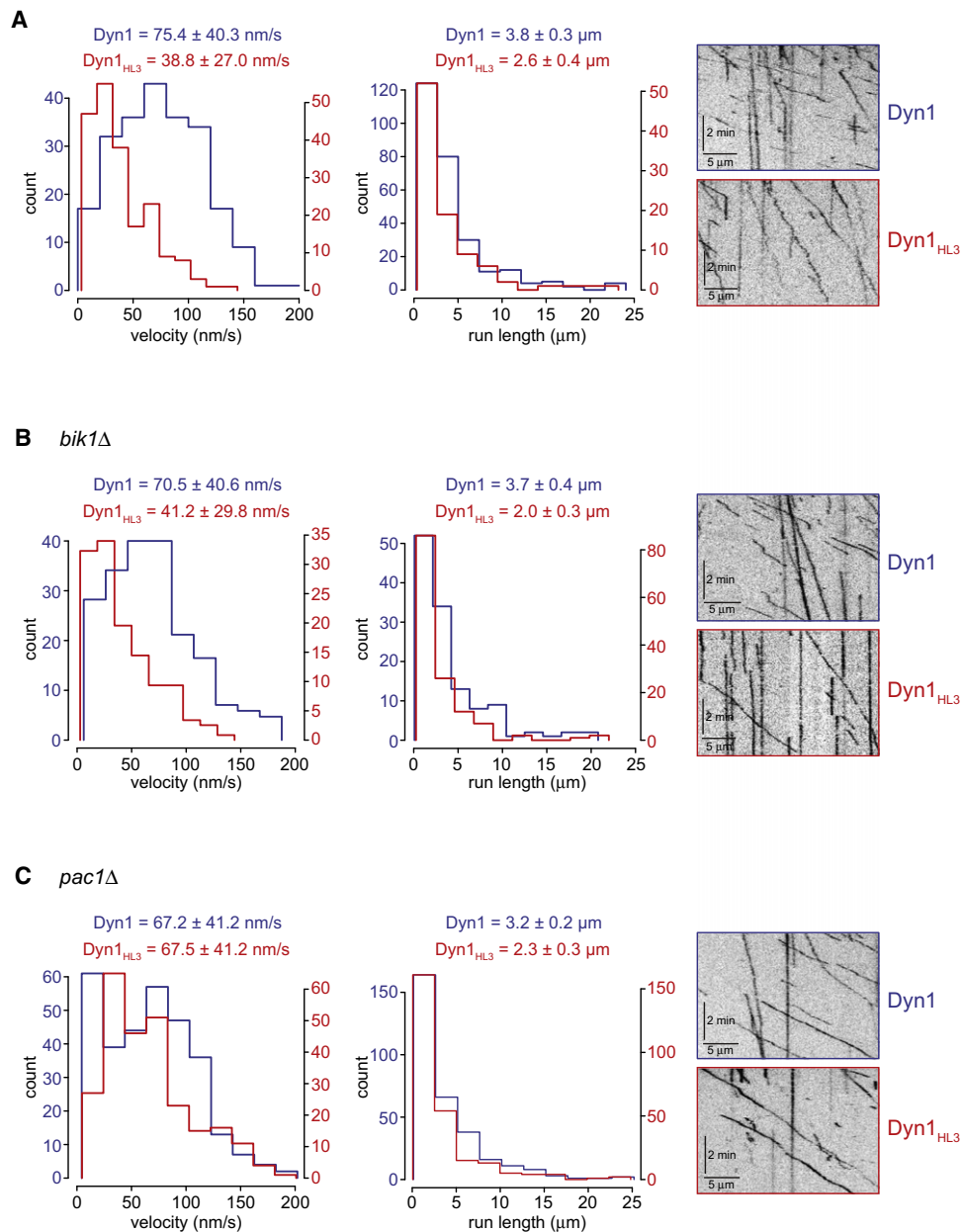


Figure 7. Dyn1_{HL3} Isolated from Cells Lacking Pac1, but Not Bik1, Exhibits Wild-Type Processive Motility

Histograms of velocities and run lengths of Dyn1 (blue) or Dyn1_{HL3} (red) isolated from (A) wild-type, (B) *bik1*Δ, or (C) *pac1*Δ strains are shown with representative kymographs from each. Single molecules of Dyn1-GFP or Dyn1_{HL3}-GFP (see Figures S6B and S6C) were visualized on taxol-stabilized rhodamine-labeled MTs using time-lapse TIRF microscopy. Mean velocities \pm standard deviation, and run lengths (determined from exponential decay fits) \pm standard error are shown for each. Only those dynein motors that moved with a velocity greater than zero were chosen for velocity and run length measurements. Also see Movies S6 and S7.

(Figure 6E), is likely responsible for reducing the velocity of this mutant. These data are consistent with the partial rescue of spindle misorientation we observed for Dyn1_{HL3} in *pac1*Δ cells (Figure 5). These data are also consistent with two recent in vitro studies, which demonstrated that LIS1 reduces the net velocity of dynein (McKenney et al., 2010; Torisawa et al., 2011). The significance of the Pac1/LIS1-mediated reduction of dynein velocity is not known; however, it is tempting to speculate that Pac1 may allow dynein to accumulate at MT plus ends

by keeping it in an “off” state, thereby allowing MT-dependent delivery to the cell cortex to consequently occur.

EXPERIMENTAL PROCEDURES

Plasmid Construction

A series of plasmids were generated to integrate various peptide sequences between the tail and motor domains of *DYN1* (between amino acids 1363 and 1364) at the native genomic locus. The motor domain defined by this

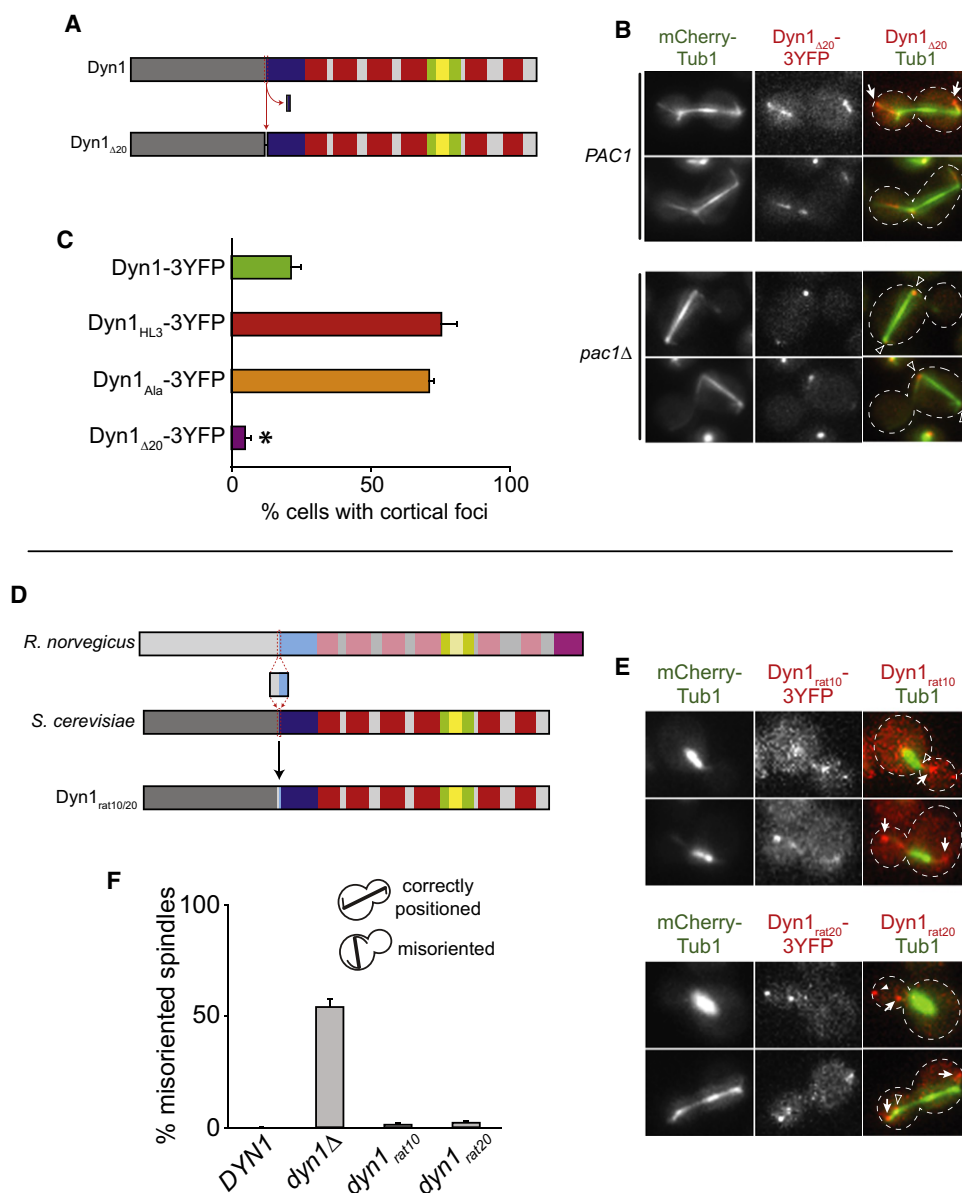


Figure 8. Differential Targeting of Dynein Elicited by Peptide Insertion, Deletion, and Substitution

(A) Schematic depicting construction of the Dyn1_{Δ20} mutant.

(B) Representative wide-field fluorescence images of *PAC1* (top) or *pac1Δ* (bottom) cells expressing mCherry-Tub1 and Dyn1_{Δ20}-3YFP. Open arrowheads show SPB foci, and arrows indicate plus end foci.

(C) The percentage of cells that exhibit cortical fluorescent foci is plotted for strains expressing mCherry-Tub1 with Dyn1-3YFP, Dyn1_{HL3}-3YFP, Dyn1_{Ala}-3YFP, or Dyn1_{Δ20}-3YFP. Stationary cortical foci were identified in two-color movies and scored accordingly. Error bars represent standard error of proportion ($n \geq 69$ cells; * $p < 0.0001$).

(D) Schematic representation of the Dyn1_{rat10} and Dyn1_{rat20} mutants (see Figure 1A for domain structure).

(E) Representative wide-field fluorescence images of cells expressing mCherry-Tub1 and either Dyn1_{rat10}-3YFP (top) or Dyn1_{rat20}-3YFP (bottom). Open arrowheads indicate SPB foci, closed arrowheads specify cortical foci, and arrows show plus end foci. Each image (in B and E) is a maximum intensity projection of a 2 μ m Z stack of wide-field images.

(F) The percentage of cells with a misoriented mitotic spindle in a cold (16°C) spindle position assay is plotted for strains carrying *DYN1* (wild-type), *dyn1Δ*, *dyn1_{rat10}*-3YFP, or *dyn1_{rat20}*-3YFP ($n \geq 217$ cells for each strain). Error bars represent standard error of proportion.

junction corresponds to the Dyn1₃₁₄ kDa construct shown to display functional motility in previous in vitro studies (Reck-Peterson et al., 2006). For a detailed discussion of the specific steps used, please see the Supplemental Experimental Procedures.

Media and Strain Construction

Strains were either derived from the protease-deficient background YWL29 (also known as BJ5457; Jones, 1990) or from YWL36 or YWL37 (Vorvis et al., 2008) and are available upon request. We transformed yeast strains

using the lithium acetate method (Knop et al., 1999). Strains carrying null mutations or fluorescently tagged components were constructed by PCR product-mediated transformation (Longtine et al., 1998) or by mating followed by tetrad dissection. Transformants were clonally purified by streaking to individual colonies on selective media. Proper tagging was confirmed by PCR. At least two independent transformants were chosen from each tagging and disruption procedure for subsequent experiments. Yeast synthetic-defined media were obtained from Sunrise Science Products (San Diego, CA, USA). A yeast genomic DNA isolation kit was obtained from Zymo Research (Orange, CA, USA). For details of strain construction methods, please see the [Supplemental Experimental Procedures](#).

Image Acquisition and Motility Assays

Yeast cultures were grown to mid-log phase at 30°C and analyzed on an agarose pad containing nonfluorescent synthetic-defined media or 50 mM potassium phosphate buffer (pH 7). Wide-field fluorescence images were collected using a 1.49 NA 100× objective on a Nikon 80i upright microscope equipped with piezo Z-control (Physik Instrumente), electronically controlled SmartShutter (Sutter Instrument), motorized filter cube turret, and a cooled EM-CCD Cascade-II camera (Photometrics). Microscope system was controlled by NIS-Elements software (Nikon). Step size of 1 μm was used to acquire Z stack images 2 μm thick. Sputtered/ET filter cube sets (Chroma Technology) were used for imaging CFP (49001), GFP (49002), YFP (49003), and mCherry (49008) fluorescence. Confocal images (Movies S1 and S2) were acquired at the University of Massachusetts Microscope Facility using a 1.49 NA 100× objective on an inverted Nikon Ti-E microscope equipped with a PerkinElmer UltraVIEW VoX and 488 nm/561 nm lasers. Step size of 0.2 μm was used to acquire Z stack images 7.2 μm thick. Three-dimensional image reconstruction was performed using ImageJ software.

The motility assay was modified from a previously described protocol (Reck-Peterson et al., 2006). Flow chambers were constructed using slides and silanized coverslips (Repel-Silane ES; GE Healthcare) attached with double-sided adhesive tape. The flow chamber was coated with anti-tubulin antibody (8 μg/ml, YL1/2; Accurate Chemical & Scientific Corporation) and then blocked with 5% Pluronic F-127 (Fisher Scientific). Taxol-stabilized MTs assembled from unlabeled and X-rhodamine-labeled bovine tubulin (10:1 ratio; Cytoskeleton) were introduced into the chamber. Following a 15 min incubation, the chamber was washed with dynein lysis buffer (see [Supplemental Experimental Procedures](#)) supplemented with 20 μM taxol, and then either Dyn1-GFP or Dyn1_{HL3}-GFP was added to the chamber. After a 2 min incubation, the chamber was washed again, and motility buffer (30 mM HEPES [pH 7.2], 50 mM potassium acetate, 2 mM magnesium acetate, 1 mM EGTA, 1 mM DTT, 1 mM Mg-ATP) supplemented with 0.05% Pluronic F-127, 20 μM taxol, and an oxygen-scavenging system (1.5% glucose, 1 U/μl glucose oxidase, 125 U/μl catalase) was added. TIRF images were collected using a 1.49 NA 100× TIRF objective on a Nikon Ti-E inverted microscope equipped with 488 nm and 561 nm 50 mW diode lasers (Coherent), a motorized TIRF illumination unit, a Perfect Focus unit with motorized nosepiece and filter cube turret (Nikon), an electronically controlled emission filter wheel (Sutter Instrument), and an iXON+ EMCCD 888 camera (Andor Technology). Microscope system was controlled by NIS-Elements software (Nikon). We used a multi-pass quad filter cube set (C-TIRF for 405/488/561/638 nm; Chroma) and emission filters mounted in the filter wheel (525/50 nm and 600/50 nm; Chroma) for imaging GFP fluorescence in the TIRF field. To collect movies of individual dynein molecules moving on MTs, we acquired frames at 2 s intervals for 8 min. Velocity and run length were determined from kymographs generated using the Multiple-Kymograph plug-in for ImageJ. For photobleaching experiments, imaging was conducted as above, except the oxygen-scavenging system was omitted, and there was no delay between exposures.

SUPPLEMENTAL INFORMATION

Supplemental Information includes seven figures, Supplemental Experimental Procedures, and seven movies and can be found with this article online at [doi:10.1016/j.devcel.2011.04.011](https://doi.org/10.1016/j.devcel.2011.04.011).

ACKNOWLEDGMENTS

We are grateful to Vladimir I. Gelfand for valuable discussion and experimental suggestions on the characterization of Dyn1_{HL3}. We thank Patricia Wadsworth for critical reading of the manuscript. We thank Jennifer Ross for generously offering the ultracentrifuge in her lab for the sucrose gradient sedimentation analysis. We are very grateful to Juan Daniel Diaz-Valencia and Leslie Conway for their help in preparing taxol-stabilized MTs and flow chambers used in the single-molecule assays. The authors wish to specially thank the editor for suggestions on editing the manuscript. This work was supported by an NIH/NIGMS grant (1R01GM076094) to W.-L.L.

Received: July 28, 2010

Revised: December 22, 2010

Accepted: April 25, 2011

Published: May 16, 2011

REFERENCES

- Adames, N.R., and Cooper, J.A. (2000). Microtubule interactions with the cell cortex causing nuclear movements in *Saccharomyces cerevisiae*. *J. Cell Biol.* 149, 863–874.
- Arai, R., Ueda, H., Kitayama, A., Kamiya, N., and Nagamune, T. (2001). Design of the linkers which effectively separate domains of a bifunctional fusion protein. *Protein Eng.* 14, 529–532.
- Burakov, A., Nadezhkina, E., Slepchenko, B., and Rodionov, V. (2003). Centrosome positioning in interphase cells. *J. Cell Biol.* 162, 963–969.
- Burgess, S.A., Walker, M.L., Sakakibara, H., Knight, P.J., and Oiwa, K. (2003). Dynein structure and power stroke. *Nature* 421, 715–718.
- Burgess, S.A., Walker, M.L., Sakakibara, H., Oiwa, K., and Knight, P.J. (2004). The structure of dynein-c by negative stain electron microscopy. *J. Struct. Biol.* 146, 205–216.
- Busson, S., Dujardin, D., Moreau, A., Dompierre, J., and De Mey, J.R. (1998). Dynein and dynactin are localized to astral microtubules and at cortical sites in mitotic epithelial cells. *Curr. Biol.* 8, 541–544.
- Cai, D., Hoppe, A.D., Swanson, J.A., and Verhey, K.J. (2007). Kinesin-1 structural organization and conformational changes revealed by FRET stoichiometry in live cells. *J. Cell Biol.* 176, 51–63.
- Carvalho, P., Gupta, M.L., Jr., Hoyt, M.A., and Pellman, D. (2004). Cell cycle control of kinesin-mediated transport of Bik1 (CLIP-170) regulates microtubule stability and dynein activation. *Dev. Cell* 6, 815–829.
- Cho, C., Reck-Peterson, S.L., and Vale, R.D. (2008). Regulatory ATPase sites of cytoplasmic dynein affect processivity and force generation. *J. Biol. Chem.* 283, 25839–25845.
- Coy, D.L., Hancock, W.O., Wagenbach, M., and Howard, J. (1999). Kinesin's tail domain is an inhibitory regulator of the motor domain. *Nat. Cell Biol.* 1, 288–292.
- Dujardin, D.L., Barnhart, L.E., Stehman, S.A., Gomes, E.R., Gundersen, G.G., and Vallee, R.B. (2003). A role for cytoplasmic dynein and LIS1 in directed cell movement. *J. Cell Biol.* 163, 1205–1211.
- Farkasovsky, M., and Kuntzel, H. (2001). Cortical Num1p interacts with the dynein intermediate chain Pac11p and cytoplasmic microtubules in budding yeast. *J. Cell Biol.* 152, 251–262.
- Friedman, D.S., and Vale, R.D. (1999). Single-molecule analysis of kinesin motility reveals regulation by the cargo-binding tail domain. *Nat. Cell Biol.* 1, 293–297.
- Gee, M.A., Heuser, J.E., and Vallee, R.B. (1997). An extended microtubule-binding structure within the dynein motor domain. *Nature* 390, 636–639.
- Grava, S., Schaerer, F., Faty, M., Philippsen, P., and Barral, Y. (2006). Asymmetric recruitment of dynein to spindle poles and microtubules promotes proper spindle orientation in yeast. *Dev. Cell* 10, 425–439.
- Hackney, D.D., Levitt, J.D., and Suhan, J. (1992). Kinesin undergoes a 9 S to 6 S conformational transition. *J. Biol. Chem.* 267, 8696–8701.

- Heil-Chapdelaine, R.A., Oberle, J.R., and Cooper, J.A. (2000). The cortical protein Num1p is essential for dynein-dependent interactions of microtubules with the cortex. *J. Cell Biol.* 151, 1337–1344.
- Hu, C.D., Chinenov, Y., and Kerppola, T.K. (2002). Visualization of interactions among bZIP and Rel family proteins in living cells using bimolecular fluorescence complementation. *Mol. Cell* 9, 789–798.
- Jones, E.W. (1990). Vacuolar proteases in yeast *Saccharomyces cerevisiae*. *Methods Enzymol.* 185, 372–386.
- Kardon, J.R., and Vale, R.D. (2009). Regulators of the cytoplasmic dynein motor. *Nat. Rev. Mol. Cell Biol.* 10, 854–865.
- Kardon, J.R., Reck-Peterson, S.L., and Vale, R.D. (2009). Regulation of the processivity and intracellular localization of *Saccharomyces cerevisiae* dynein by dynactin. *Proc. Natl. Acad. Sci. USA* 106, 5669–5674.
- Knop, M., Siegers, K., Pereira, G., Zachariae, W., Winsor, B., Nasmyth, K., and Schiebel, E. (1999). Epitope tagging of yeast genes using a PCR-based strategy: more tags and improved practical routines. *Yeast* 15, 963–972.
- Kobayashi, T., and Murayama, T. (2009). Cell cycle-dependent microtubule-based dynamic transport of cytoplasmic dynein in mammalian cells. *PLoS One* 4, e7827.
- Krementsov, D.N., Kremntsova, E.B., and Trybus, K.M. (2004). Myosin V: regulation by calcium, calmodulin, and the tail domain. *J. Cell Biol.* 164, 877–886.
- Lampert, F., Hornung, P., and Westermann, S. (2010). The Dam1 complex confers microtubule plus end-tracking activity to the Ndc80 kinetochore complex. *J. Cell Biol.* 189, 641–649.
- Lee, W.L., Oberle, J.R., and Cooper, J.A. (2003). The role of the lissencephaly protein Pac1 during nuclear migration in budding yeast. *J. Cell Biol.* 160, 355–364.
- Lee, W.L., Kaiser, M.A., and Cooper, J.A. (2005). The offloading model for dynein function: differential function of motor subunits. *J. Cell Biol.* 168, 201–207.
- Li, J., Lee, W.L., and Cooper, J.A. (2005). NudEL targets dynein to microtubule ends through LIS1. *Nat. Cell Biol.* 7, 686–690.
- Lin, H., de Carvalho, P., Kho, D., Tai, C.Y., Pierre, P., Fink, G.R., and Pellman, D. (2001). Polyploids require Bik1 for kinetochore-microtubule attachment. *J. Cell Biol.* 155, 1173–1184.
- Longtine, M.S., McKenzie, A., 3rd, Demarini, D.J., Shah, N.G., Wach, A., Brachat, A., Philippsen, P., and Pringle, J.R. (1998). Additional modules for versatile and economical PCR-based gene deletion and modification in *Saccharomyces cerevisiae*. *Yeast* 14, 953–961.
- Markus, S.M., Punch, J.J., and Lee, W.L. (2009). Motor- and tail-dependent targeting of dynein to microtubule plus ends and the cell cortex. *Curr. Biol.* 19, 196–205.
- Markus, S.M., Plevock, K.M., St Germain, B.J., Punch, J.J., Meaden, C.W., and Lee, W.L. (2011). Quantitative analysis of Pac1/LIS1-mediated dynein targeting: implications for regulation of dynein activity in budding yeast. *Cytoskeleton (Hoboken)* 68, 157–174.
- McKenney, R.J., Vershinin, M., Kunwar, A., Vallee, R.B., and Gross, S.P. (2010). LIS1 and NudE induce a persistent dynein force-producing state. *Cell* 141, 304–314.
- Meng, X., Samsó, M., and Koonce, M.P. (2006). A flexible linkage between the dynein motor and its cargo. *J. Mol. Biol.* 357, 701–706.
- Mocz, G., and Gibbons, I.R. (2001). Model for the motor component of dynein heavy chain based on homology to the AAA family of oligomeric ATPases. *Structure* 9, 93–103.
- Moore, J.K., Li, J., and Cooper, J.A. (2008). Dynactin function in mitotic spindle positioning. *Traffic* 9, 510–527.
- Nishiura, M., Kon, T., Shiroguchi, K., Ohkura, R., Shima, T., Toyoshima, Y.Y., and Sutoh, K. (2004). A single-headed recombinant fragment of *Dictyostelium* cytoplasmic dynein can drive the robust sliding of microtubules. *J. Biol. Chem.* 279, 22799–22802.
- Pasternak, C., Flicker, P.F., Ravid, S., and Spudich, J.A. (1989). Intermolecular versus intramolecular interactions of *Dictyostelium* myosin: possible regulation by heavy chain phosphorylation. *J. Cell Biol.* 109, 203–210.
- Reck-Peterson, S.L., Yildiz, A., Carter, A.P., Gennerich, A., Zhang, N., and Vale, R.D. (2006). Single-molecule analysis of dynein processivity and stepping behavior. *Cell* 126, 335–348.
- Seiler, S., Kirchner, J., Horn, C., Kallipolitou, A., Woehlke, G., and Schliwa, M. (2000). Cargo binding and regulatory sites in the tail of fungal conventional kinesin. *Nat. Cell Biol.* 2, 333–338.
- Sheeman, B., Carvalho, P., Sagot, I., Geiser, J., Kho, D., Hoyt, M.A., and Pellman, D. (2003). Determinants of *S. cerevisiae* dynein localization and activation: implications for the mechanism of spindle positioning. *Curr. Biol.* 13, 364–372.
- Stock, M.F., Guerrero, J., Cobb, B., Eggers, C.T., Huang, T.G., Li, X., and Hackney, D.D. (1999). Formation of the compact conformation of kinesin requires a COOH-terminal heavy chain domain and inhibits microtubule-stimulated ATPase activity. *J. Biol. Chem.* 274, 14617–14623.
- Stoffler, H.E., and Bahler, M. (1998). The ATPase activity of Myr3, a rat myosin I, is allosterically inhibited by its own tail domain and by Ca²⁺ binding to its light chain calmodulin. *J. Biol. Chem.* 273, 14605–14611.
- Torisawa, T., Nakayama, A., Furuta, K., Yamada, M., Hirotsune, S., and Toyoshima, Y.Y. (2011). Functional dissection of LIS1 and NDEL1 towards understanding the molecular mechanism of cytoplasmic dynein regulation. *J. Biol. Chem.* 286, 1959–1965.
- Verhey, K.J., Lizotte, D.L., Abramson, T., Barenboim, L., Schnapp, B.J., and Rapoport, T.A. (1998). Light chain-dependent regulation of Kinesin's interaction with microtubules. *J. Cell Biol.* 143, 1053–1066.
- Vorvis, C., Markus, S.M., and Lee, W.L. (2008). Photoactivatable GFP tagging cassettes for protein-tracking studies in the budding yeast *Saccharomyces cerevisiae*. *Yeast* 25, 651–659.
- Wang, F., Thirumurugan, K., Stafford, W.F., Hammer, J.A., 3rd, Knight, P.J., and Sellers, J.R. (2004). Regulated conformation of myosin V. *J. Biol. Chem.* 279, 2333–2336.
- Whyte, J., Bader, J.R., Tauhata, S.B., Raycroft, M., Hornick, J., Pfister, K.K., Lane, W.S., Chan, G.K., Hinchcliffe, E.H., Vaughan, P.S., et al. (2008). Phosphorylation regulates targeting of cytoplasmic dynein to kinetochores during mitosis. *J. Cell Biol.* 183, 819–834.
- Woodruff, J.B., Drubin, D.G., and Barnes, G. (2009). Dynein-driven mitotic spindle positioning restricted to anaphase by She1p inhibition of dynactin recruitment. *Mol. Biol. Cell* 20, 3003–3011.